An experimental study of the breakage of liquid bridges at stability limit of minimum volume

J. L. Espino, J. Meseguer, and A. Laverón-Simavilla
IDR/UPM, E.T.S.I. Aeronáuticos, Universidad Politécnica de Madrid, E-28040 Madrid, Spain

(Received 7 June 2002; accepted 22 July 2002; published 5 September 2002)

An experimental apparatus to study the breaking process of axisymmetric liquid bridges has been developed, and the breaking sequences of a large number of liquid bridge configurations at minimum-volume stability limit have been analyzed. Experimental results show that very close to the breaking moment the neck radius of the liquid bridge varies as $t^{1/3}$, where t is the time to breakage, irrespective of the value of the distance between the solid disks that support the liquid column. © *2002 American Institute of Physics.* [DOI: 10.1063/1.1506312]

I. INTRODUCTION

The liquid bridge is here considered as an isothermal mass of liquid with constant properties (density, ρ, surface tension, σ, and viscosity, μ) held by surface tension forces between two parallel and coaxial circular disks of the same radii R, placed at a distance L apart (as sketched in Fig. 1). The axis of symmetry of the liquid column is aligned with the gravity acceleration, g. The liquid bridge interface is anchored to the disks, being the two contact lines circles pinned to the edges of the disks.

Equilibrium shapes and stability limits of the fluid configuration are defined by the following dimensionless parameters: The slenderness $\Lambda = L/(2R)$, the dimensionless volume of liquid $V = V^*/(\pi R^2 L)$, where V^* stands for the physical volume, and the axial Bond number $B = (\rho - \rho_s) g R^2/\sigma$, being ρ_s the density of the surrounding medium (which is assumed to have constant and uniform properties, and also for air surrounding $\rho_s \ll \rho$). For a weightless right circular cylinder liquid bridge the well-known Rayleigh stability limit holds: The liquid column becomes unstable when its length is larger than its circumference ($\Lambda > \pi$). Many perturbations to this ideal configuration, involving different geometrical configurations and several arrangements of the supporting disks as well as nonaxial acceleration, have been analyzed (a review on this topic can be found in Meseguer *et al.*[1]). The stability limits of the liquid bridge configurations here considered (in which the only parameters involved are L, V, and B) were extensively analyzed by Slobozhanin and Perales,[2] where stability limits for a wide range of values of the Bond number are presented.

The stability limit obtained with static considerations for $B = 0$ can be either a turning point or a bifurcation point depending on the slenderness of the liquid bridge,[3] and the corresponding eigenfunction is either symmetric or antisymmetric. The slenderness therefore determines the symmetry or nonsymmetry (with respect to the middle plane parallel to the disks) of the unstable equilibrium shapes, being symmetric those corresponding to $\Lambda < \Lambda_A$, and nonsymmetrical for $\Lambda > \Lambda_A$, where $\Lambda_A = 2.128$.

The behavior is similar when $B \neq 0$, and it has been numerically demonstrated[4,5] that symmetric or nonsymmetric effects are the dominant ones in the breaking dynamics depending on the value of the slenderness.

The study of nonlinear dynamics and breakage of liquid bridges was started more than twenty years ago, using an inviscid, one-dimensional slices model.[4–9] This initial model was developed from one used in capillary jet studies, just modifying the boundary condition. Sirignano and Mehring[10] have recently published a wide review of the theories commonly used in liquid jet breaking, and an historical review of the more representative publications concerning the breaking of liquid bridges can be found in Zhang, Padgett, and Basaran.[11] This list of publications should be completed with the last published papers on this topic, which are mainly devoted to the breaking of stretching liquid bridges[11–14] and liquid bridges held between spherical supports.[15,16]

In the case of stretching liquid bridges, Yildirim and Basaran[13] have demonstrated with numerical calculations that at the end of the breaking process of low viscosity liquid bridges, very near to the rupture, the minimum liquid bridge radius R_n varies with the time to breakup t as $R_n \sim t^{2/3}$ (potential flow scaling regime), whereas even closer to the breaking instant the neck radius behaves as $R_n \sim t$ (inertial-viscous threat regime). However, in the case of liquid bridges held between fixed disks, earlier numerical results[4–8] indicate that, very close to the breakage, the neck radius of the liquid bridge behaves as $R_n \sim t^{1/3}$. Aiming to check this discrepancy, an experimental apparatus has been developed, and several sets of experiments dealing with the breaking dynamics of liquid bridges at minimum-volume stability limits have been performed.

II. APPARATUS

The experimental set-up used to perform the experiments concerning the breaking dynamics of liquid bridges, as shown in Fig. 2, consists of the following main elements: Liquid bridge cell (A), microscope (B), high speed video camera (C), standard rate CCD camera (D), illumination system (E), image recording system (not shown in the figure) and associated image processing software.

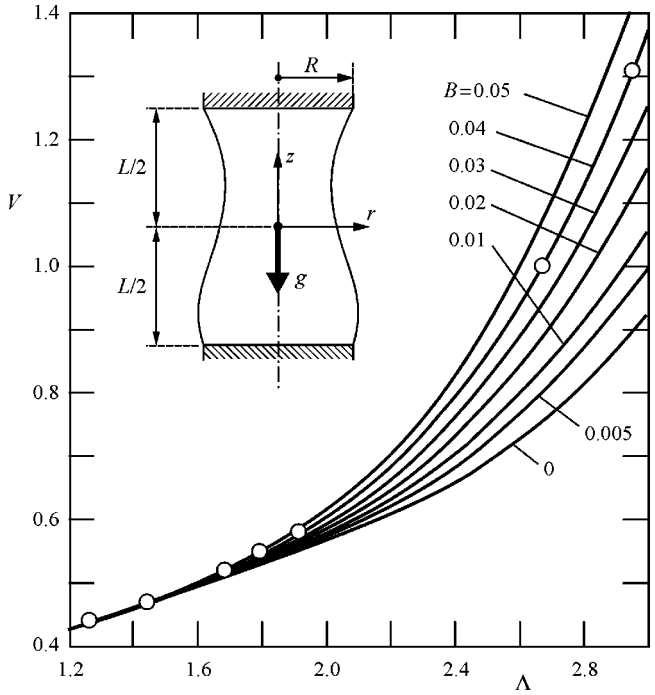

FIG. 1. Liquid bridge setup and variation of the minimum-volume stability limits with the Bond number, B, in the Λ-V plane (slenderness-dimensionless volume). Symbols represent experimental configurations tested (all for $B=0.04$).

The liquid bridge cell is a small block of aluminum with three cylindrical holes whose axes are aligned with the reference system axes. The vertical drilled hole, 3 mm in diameter, allows the displacement of two cylinders of the same diameter. These cylinders are drilled along their axes, where two small stainless steel calibrated-diameter cylinders are located. The calibrated-diameter small cylinders that support the liquid bridge are solid rods 1 mm in diameter. The flat surfaces in contact with the liquid have been carefully polished in order to obtain very sharp edges. The two horizontal holes define two perpendicular viewing axis of the virtual chamber where the liquid bridge is formed.

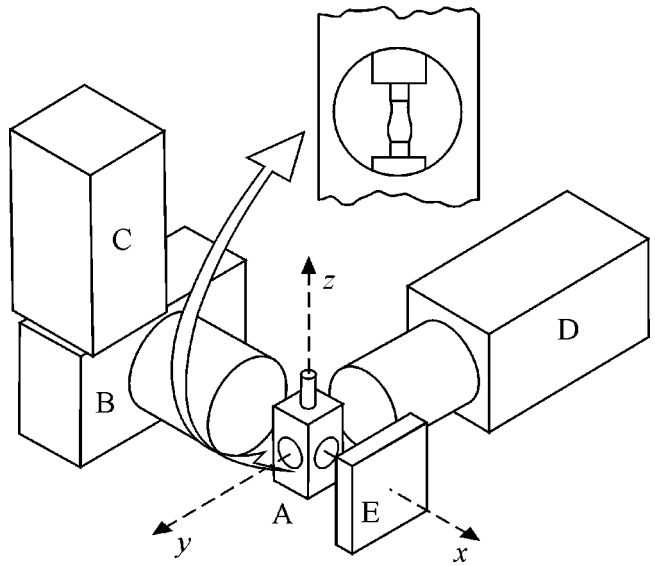

FIG. 2. Experimental setup: liquid bridge cell (A), microscope (B), high-speed video camera (C), standard rate CCD camera (D), and illumination system (E).

Liquid bridges are formed directly by placing a drop of working liquid (distilled water) between both supporting disks with a calibrated syringe (Hamilton Microliter Syringe 801 RNE).

There are two CCD cameras mounted on the platform, one of them with its optical axis aligned with the x axis of the liquid bridge cell, whereas the optical axis of the second one is oriented in the direction of the y axis. The x axis CCD camera is a high-speed camera (HISIS 2002) which can record up to 2400 frames per second. Most of the breaking sequences have been recorded at 1220 images per second, at a resolution of 256×256 pixels, which is the maximum recording speed for which full resolution images can be taken (the resolution is halved for the higher recording speed). The x axis high speed CCD camera is mounted on a microscope (WILD M8) to have a frame covering some 6 mm by 6 mm. The second CCD camera, a SONY CCD-IRIS, is used to provide to the operator enlarged images of the liquid bridge in a more user-friendly format, through the corresponding TV monitor (high speed frames can be observed mainly off-line). The last mentioned images are used to detect the moment when the breaking of the liquid bridge takes place, at which the high-speed video camera is stopped (a buffer is storing continuously the last 8 s of the high speed recording).

The illumination system consists of a background LED stroboscope (9 LEDs arranged in a matrix of 3 by 3) driven by the HISIS 2002 system. The stroboscope illuminates the liquid column from the rear (as seen from the high speed camera), so that the liquid–air interface becomes sharply contrasted (the liquid column, and specially its edges, turns out very dark since the liquid bridge acts like a small lens).

III. EXPERIMENTAL RESULTS

The experimental procedure is as follows: once the supporting rods are installed with their longitudinal axes aligned, the upper rod is placed a given distance apart from the lower one. Then a drop of water is formed at the tip of the feeding tube of the calibrated syringe, and the tip of this feeding needle is carefully displaced until the drop comes into contact with the supporting rods and a liquid bridge is formed. Usually the liquid column perfectly anchors to the edges of the rods, due to the sharpness of their edges, and it is quite unusual to spread the liquid over the lateral surfaces of the supporting rods during the liquid bridge formation. In all the cases the amount of liquid supplied to the liquid bridge is large enough to ensure that the volume of the initial drop is far enough from the minimum-volume stability limit corresponding to the selected slenderness.

Once the liquid bridge is formed, the experimental sequence proceeds without any further interaction: Due to the evaporation the volume of liquid continuously decreases and the liquid column breaks when the stability limit is reached. In all the process, direct manipulation on the liquid bridge cell is prevented in order to avoid vibrations that could cause the unexpected breaking of the liquid column before the cor-

responding stability limit is reached. Several tests have been performed to determine the evaporation rate, dV/dt, during the experiments, the results obtained being $dV/dt \approx 1.8 \times 10^{-3}\ s^{-1}$ (note that V is the dimensionless volume).

All along the breaking sequence, liquid bridge pictures obtained from HISIS 2002 CCD camera, at a rate of 1220 frames per second, are stored in a system internal buffer. When the operator realizes that the breakage of the liquid column occurs, the recording process is stopped, and the buffered breaking sequence is transferred to the PC for further analysis. About two hundred frames prior to breaking time are selected and stored together with a high enough number of images taken after the breaking instant. The same process, maintaining the distance between the disks, is repeated at least four times to check the repeatability of measurements. Afterwards a new value of the slenderness is set, and the whole process is repeated.

The Bond number, B, for each experiment is calculated analyzing the interface deformation of the liquid bridge when its dimensionless volume is near to $V=1$. This procedure has already been used in previous experimental studies.[17] Since liquid bridges are formed with an initial volume larger than that of the cylinder ($V>1$), there are always several images of the liquid bridge with almost cylindrical volume ($V \approx 1$) during the breaking sequence, images which are selected, stored and digitized. For each image the volume of the liquid bridge is computed from the digitized outer shapes. When the volume is within the range $V=1\pm0.005$ the value of the Bond number is calculated by fitting a linear order theoretical expression for the interface shape experimentally measured. The same procedure has been repeated several times along the experimental campaign (using different values of the slenderness) in order to check that surface tension does not change during experiments, all results obtained being $B=0.040\pm0.001$ (for liquid bridges between disks having 0.50 mm in radius). This value is very close to the value of reference ($B=0.034$), which would be obtained by taking the nominal values of the physical magnitudes entering the definition of the Bond number ($g=9.81\ m.s^{-2}$, $\rho=10^3\ kg.m^{-3}$, and $\sigma=0.073\ N.m^{-1}$). The small difference is thought to be due to the decrease in the value of the surface tension, due to interface contamination or to geometrical inaccuracies not accounted for in calculations.

The experimental configurations tested are represented in the Λ-V stability diagram (Fig. 1) along with several analytical stability limit curves corresponding to different values of the Bond number. All experimental points obviously lay over the nominal stability limit curve for the measured Bond number ($B=0.040$).

Experimental results of the variation of the relative neck radius, r, with the breakage time, t, are shown in Fig. 3. Relative dimensionless neck radius r is defined as the ratio, $r=R_n/R$, of the radius at the neck of the liquid column, R_n, to the radius of the supporting rods, R. The low scattering of experimental data ensures repeatability of the experimental procedure (different runs were plotted with the same symbol for a given slenderness). It should be pointed out that the breaking process is more violent as the slenderness decreases, which can be explained by taking into account that the mass of the liquid column (hence inertial effects) decreases as the slenderness decreases, therefore, the capillary effects are of greater importance as the length of the liquid column diminishes.

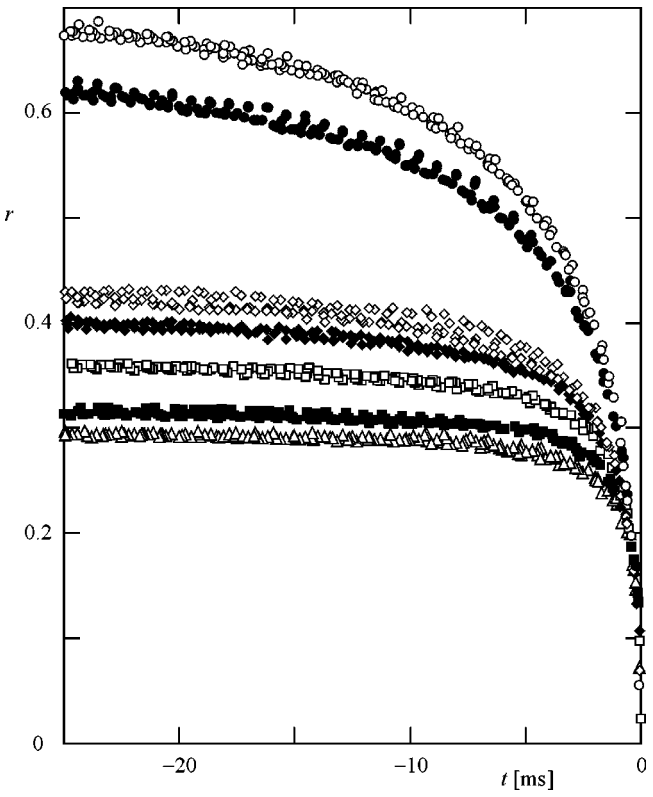

FIG. 3. Variation of the relative neck radius, r, with the time to the liquid bridge breakage, t. Symbols identify the liquid bridge slenderness according to the following key: $\Lambda=2.95$ (white circles), $\Lambda=2.67$ (black circles), $\Lambda=1.92$ (white rhombi), $\Lambda=1.80$ (black rhombi), $\Lambda=1.69$ (white squares), $\Lambda=1.45$ (black squares), $\Lambda=1.27$ (white triangles).

To analyze the dependence of the relative neck radius, r, with the time to the breaking instant, t, the same data already represented in Fig. 3 are plotted in Fig. 4 using logarithmic

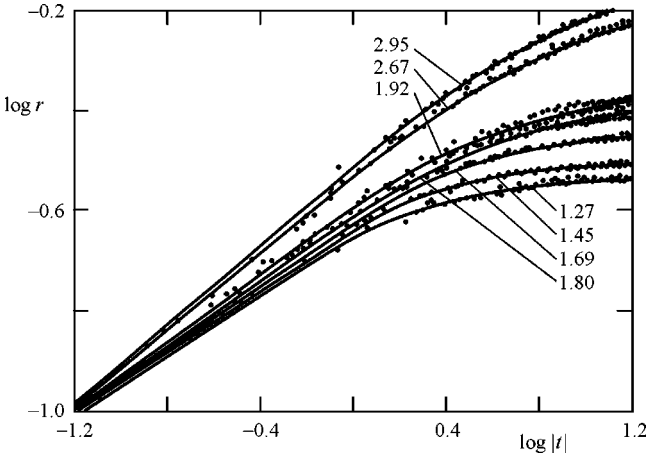

FIG. 4. Variation of logarithm of the relative neck radius, $\log r$, with the logarithm of the time to liquid bridge breakage, $\log|t|$. Symbols represent experimental results. Numbers on the curves identify the value of the slenderness Λ.

scales. As expected, for large values of the time, t, the different sets of data are grouped around almost horizontal lines (these would be truly horizontal lines if the evaporation effects were not present). However, for very small values of t, all experimental points lie in a narrow band limited by straight lines whose slopes range between $n=0.3$ and $n=0.4$, the average value being $n=1/3$. This seems to indicate that very close to breaking, the neck radius behaves as $r \sim t^{1/3}$, as already predicted by numerical analysis,[4–8] whereas in the case of stretching liquid bridges the scaling law reported by Yildirim and Basaran[13] is $r \sim t$. In the last case the necking is forced by the displacement of one of the supporting disks, so that one could expect a faster variation of the neck radius at the end of the breaking process.

Finally, it must be pointed out that in all the tested configurations a satellite droplet have always been observed when the breaking of the liquid column takes place, no matter the value of the slenderness.

ACKNOWLEDGMENT

The authors are indebted to Professor J. M. Perales for helpful discussions.

[1] J. Meseguer, J. M. Perales, I. Martínez, N. A. Bezdenejnykh, and A. Sanz, "Hydrostatic instabilities in floating zone crystal growth process," Curr. Top. Cryst. Growth Res. **5**, 27 (1999).
[2] L. A. Slobozhanin and J. M. Perales, "Stability of liquid bridges between equal disks in an axial gravity field," Phys. Fluids A **5**, 1305 (1993).
[3] I. Martinez, "Stability of axisymmetric liquid bridges," Proc. 4th European Symp. Mat. Sci. Microgravity, ESA SP-191, 267 (1983).
[4] J. Meseguer, A. Sanz, and D. Rivas, "The breaking of axisymmetric non-cylindrical liquid bridges," Proc. 4th European Symp. Mat. Sci. Microgravity, ESA SP-191, 261 (1983).
[5] J. Meseguer and A. Sanz, "Numerical and experimental study of the dynamics of axisymmetric slender liquid bridges," J. Fluid Mech. **153**, 83 (1985).
[6] J. Meseguer, "The breaking of axisymmetric slender liquid bridges," J. Fluid Mech. **130**, 123 (1983).
[7] J. Meseguer, "The influence of axial gravity on the breakage of axisymmetric slender liquid bridges," J. Cryst. Growth **62**, 577 (1983).
[8] J. Meseguer, "The dynamics of axisymmetric slender liquid bridges between unequal disks," J. Cryst. Growth **73**, 599 (1985).
[9] D. Rivas and J. Meseguer, "One-dimensional, self similar solution of the dynamics of axisymmetric slender liquid bridges," J. Fluid Mech. **138**, 417 (1984).
[10] W. A. Sirignano and C. Mehring, "Review of theory of distortion and disintegration of liquid streams," Prog. Energy Combust. Sci. **26**, 609 (2000).
[11] X. Zhang, R. S. Padgett, and O. A. Basaran, "Nonlinear deformation and breakup of stretching liquid bridges," J. Fluid Mech. **329**, 207 (1996).
[12] J. F. Padday, G. Pétré, C. G. Rusu, J. Gamero, and G. Wozniak, "The shape, stability and breakage of pendant liquid bridges," J. Fluid Mech. **352**, 177 (1997).
[13] O. E. Yildirim and O. A. Basaran, "Deformation and breakup of stretching bridges of Newtonian and shear-thinning liquids: comparison of one- and two-dimensional models," Chem. Eng. Sci. **56**, 211 (2001).
[14] B. Ambravaneswaran and O. A. Basaran, "Effects of insoluble surfactants on the nonlinear deformation and breakup of stretching liquid bridges," Phys. Fluids **11**, 997 (1999).
[15] Z. Lai and S. Lu, "Liquid bridge rupture criterion between spheres," Int. J. Min. Process. **53**, 171 (1998).
[16] O. Pitois, P. Moucheront, and X. Chateau, "Liquid bridge between two moving spheres: an experimental study of viscosity effects," J. Colloid Interface Sci. **231**, 26 (2000).
[17] J. Meseguer, N. A. Bezdenejnykh, J. M. Perales, and P. Rodríguez de Francisco, "Theoretical and experimental analysis of stability limits of nonaxisymmetric liquid bridges under microgravity conditions," Microgravity Sci. Technol. **8**, 2 (1995).